In Vivo Demonstration of Single Transducer Harmonic Motion Imaging (ST-HMI) in a Breast Cancer Mouse Model and Breast Cancer Patients

Md Murad Hossain
Department of Biomedical Engineering
Columbia University
New York, USA
mh4051@columbia.edu

Niloufar Saharkhiz
Department of Biomedical Engineering
Columbia University
New York, USA
ns3149@columbia.edu

Elisa E. Konofagou
Department of Biomedical Engineering
Columbia University
New York, USA
ek2191@columbia.edu

***Abstract*—Harmonic motion imaging (HMI) interrogates the mechanical properties of tissues by simultaneously generating and tracking amplitude-modulated (AM) force-induced motion using focused ultrasound and imaging transducers, respectively. The main advantages of HMI are that motion at oscillation frequency can be easily filtered from different motion artifacts. However, the current configuration of two separate transducers renders the HMI system highly complex. The objective of this study is to develop a single transducer HMI (ST-HMI) and test its feasibility of generating and mapping of harmonic motion using a linear array transducer to facilitate data acquisition. The feasibility of ST-HMI was performed by imaging commercially available two elastic phantoms with two inclusions (N=4), *in vivo* monitoring of changes in the tumor stiffness of 4T1, orthotropic breast cancer mouse model, and patient with invasive ductal carcinoma (IDC) breast cancer. ST-HMI-derived peak-to-peak displacements (P2PD) successfully contrasted all 4 inclusions with nominal Young's modulus of 8, 10, 40, and 60 kPa and the P2PD ratio of background to inclusion was highly correlated with Young's modulus ratio of inclusion to background with R^2 of 0.93. In the mouse study, the median P2PD ratio of the tumor to non-cancerous tissue was 2.0, 3.6, 7.0, and 6.6 at 1, 2, 3, and 4 weeks, respectively, post-injection of the tumor cell. In the clinical study, ST-HMI detected IDC cancer with the P2PD ratio of 1.78. These results indicate that ST-HMI can assess the mechanical properties of tissues via generation and tracking of harmonic motion using a single transducer.**

Keywords— Harmonic motion imaging; Acoustic radiation force; Elasticity imaging; Breast Cancer; Ultrasound.

I. Introduction

Mechanical properties of tissues are diagnostically relevant given that diseases and pathology change the underlying mechanical properties of tissues. Over the past three decades, ultrasonic methods [1] for interrogating tissue mechanical properties have been extensively studied and applied to diagnose diseases in liver [2], breast [3], thyroid [4], prostate [5], kidney [6], [7], muscles [8], carotid artery [9], and lymph nodes [10].

Among the various UE approaches are those that exploit acoustic radiation force (ARF) [1] to induce motion within the tissue. ARF-induced motion at "on-axis" to the ARF region of excitation (ROE) or ARF-induced shear wave velocity "off-axis" to the ARF ROE can be used to assess mechanical properties [1]. One of the "on-axis" ARF-based methods to interrogate mechanical properties is harmonic motion imaging (HMI) [11]. The main difference between HMI with other "on-axis" based methods is that amplitude modulated (AM)-ARF (AM-ARF) is used to generate harmonic oscillation of tissue whereas other "on-axis" methods use pulsed ARF. The advantage of using harmonic excitation is the fact that motion at the input oscillation frequency can be easily filtered from reverberation, body movements, and breathing artifacts. Previously, HMI has been used for detecting pancreatic tumors [12], monitoring treatment response of pancreatic tumors [13], monitoring of high intensity focused ultrasound-induced ablation of tumors [14], [15], and livers [16]. In the current HMI configuration, a focused ultrasound (FUS) and an imaging transducer simultaneously generate and track AM-ARF-induced motion respectively, and a 2-D image is generated by mechanically translating both transducers. The current use of two different transducers with a mechanical positioner to generate a 2-D image renders the HMI system highly complex to use for diagnostic imaging. The data acquisition would be facilitated if the generation and tracking of harmonic motion could be performed by a single imaging transducer with electronic steering for generating 2-D image.

Towards the goal of facilitating HMI data acquisitions, this study investigates the feasibility of generating and mapping harmonic motion using a linear array transducer. This new HMI method, named single transducer-HMI (ST-HMI), generates AM-ARF by modulating the excitation pulse duration and estimates motion by collecting tracking pulses in between the excitation pulses. The feasibility of ST-HMI is hereby tested by imaging commercially available elastic phantoms with cylindrical inclusions, *in vivo* breast cancer mouse model, and *in vivo* breast cancer patients.

II. Materials and Methods

A. Single Transducer Harmonic Motion Imaging Excitation and Tracking Pulse Sequence

In ST-HMI, AM-ARF was generated by sinusoidally varying excitation pulse duration (i.e cycle number) and tracking pulses were collected in between excitation pulses to estimate the induced displacements. Fig. 1 shows excitation (red) and tracking (blue) pulse sequence for one-period oscillation with frequency and excitation pulse per cycle of 200 Hz and 8, respectively. Tracking pulses were like typical 2-cycle B-mode imaging pulse whereas excitation pulses are long duration pulse. Note, tissue displacement linearly increases with excitation pulse duration for fixed acoustic pressure [17]. So, sinusoidal variation in excitation pulse duration generates sinusoidally modulated displacements. This pulse sequence was repeated to

This work was supported by NIH under Grant R01 CA228275.

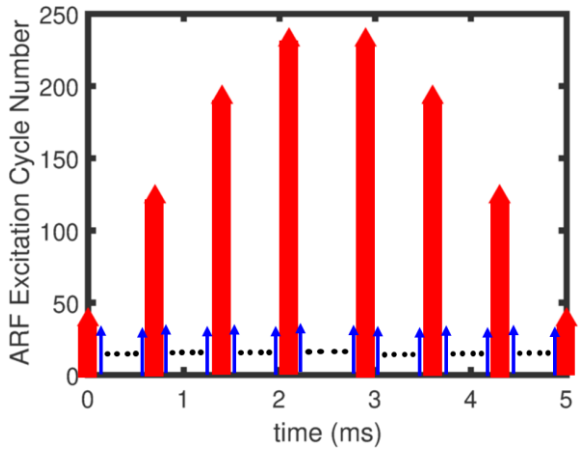

Fig. 1: ST-HMI pulse sequence with the excitation pulse cycle number (red) and tracking pulse (blue) for 200-Hz oscillation frequency and 8 excitation pulses per cycle. The excitation pulse cycle number is variable to generate amplitude-modulated force whereas the tracking pulse cycle number is fixed to 2. The excitation and tracking pulses were not drawn to the scale.

generate 5 cycles of oscillation at each lateral line. A reference tracking pulse was collected before the 1st excitation pulse and the motion was estimated with respect to the reference pulse.

B. Phantom Experiments

Imaging of two commercially available phantoms (customized model 049A, CIRS, Norfolk, VA) was performed using a Verasonics research system (Vantage 256, Verasonics Inc., Kirkland, WA, USA) with L7-4 transducer (Philips Healthcare, Andover, MA, USA). In both phantoms, two stepped-cylindrical inclusions with varying diameters and stiffness were embedded in a 5 ± 1.0 kPa background. The manufacturer-provided Young's modulus of 4 inclusions was 8 ± 1.5, 10 ± 2, 40 ± 8, and 60 ± 10. Imaging was performed at 10 ± 1.0 mm cross-section of the cylindrical inclusions. In all inclusions, ST-HMI was performed using oscillation frequency, excitation pulse number per cycle, and oscillation cycle number of 220 Hz, 8, and 5, respectively. The center frequency of excitation and tracking pulse was 4.0 and 6.1 MHz with F-number of 2.25 and 1.75, respectively. The axial focal depth was fixed to 15 mm with a pulse repetition frequency of 10 kHz. For two-dimensional imaging, 34 evenly spaced A-lines were acquired across approximately 20 mm lateral FOV. Preceding each 2-D ST-HMI acquisition was one spatially-matched B-mode image, with 128 lateral lines spanning a lateral FOV of approximately 38 mm, for anatomical reference.

C. Imaging of In Vivo breast cancer mouse model

An orthotropic, 4T1 breast cancer mouse model was used to investigate the performance of ST-HMI in monitoring longitudinal changes in tumor stiffness. Induction of cancer and imaging protocols were reviewed and approved by the Columbia University Irving Medical Center (CUIMC) Institutional Animal Care and Use Committee (IACUC). Eight to ten-week-old female BALB/c mice were purchased from the Jackson Laboratory. Cancer was inducted by injecting 2 x 10^5 4T1 breast cancer cells in the 4th inguinal mammary fat pad [18]. The experimental set up similar to the Payen et al. [19] was used. Mice were imaged using the same Verasonics research system with L22-14vXLF (Vermon, Tours, France) linear array at 1, 2, 3, and 4 weeks post-injection of tumor cell. ST-HMI was performed using oscillation frequency, excitation pulse number per cycle, and oscillation cycle number of 200 Hz, 13, and 5, respectively. The center frequency of excitation and tracking pulse was 15.6 and 20.8 MHz with F-number of 2.25 and 1.75, respectively. The axial focal depth was varied from 11 to 15 mm depending on the size of the tumor. 2-D HMI image was formed by acquiring fourteen evenly spaced A-lines across 4 mm lateral FOV. One spatially-matched B-mode image was acquired with 128 lateral lines spanning a lateral FOV of approximately 13.6 mm, for anatomical reference.

D. Imaging of Breast Cancer Patient

Clinical performance of ST-HMI was evaluated by imaging a female invasive ductal carcinoma cancer patient following human subjects protocol approval by the CUIMC Institutional Review Board (IRB). Informed consent was obtained from the patient. Similar to the phantom experiments, ST-HMI was performed using the same Verasonics research system with an L7-4 linear array. Patients were imaged in a supine or lateral oblique position and the location and boundaries of tumors were confirmed by an experienced sonographer in the B-mode ultrasound image. Data were collected by orienting transducer parallel to the radial direction (i.e., line connecting center of mass and nipple).

E. Single Transducer Harmonic Motion Imaging Data Processing

For all acquisitions, channel data were transferred to the computational workstation for offline processing using MATLAB (MathWorks Inc., Natick, MA, USA). Custom delay and sum beamforming was applied to construct beamformed RF data. Motion tracking with respect to the reference tracking pulse was performed using one-dimensional normalized cross-correlation (NCC) [20]. At each spatial location (axial x lateral), the differential displacements were computed by subtracting displacements between successive time samples. Then, the desired oscillation was filtered out using a second-order Butterworth bandpass filter (*butter* and *filter* function). After filtering out the desired oscillations, a 2-D image was formed by calculating average peak-to-peak displacement (P2PD) over cycles for each pixel. The P2PD is a function of the ARF amplitude which varies over the axial range. So, the depth-dependent variation in P2PD must be normalized before P2PD can be compared over the axial range. Normalization was performed using the method described in Hossain et al. [21].

III. Results and Discussions

Fig. 2 qualitatively compares the normalized P2PD images of 8, 10, 40, and 60 kPa inclusions embedded in 5 kPa background. The inclusion contrast increased with Young's modulus of the inclusion which is expected. The P2PD ratios of background to inclusion were 1.2, 1.6, 5.4, and 5.8 in 8, 10, 40, and 60 kPa inclusions, respectively, and were highly correlated with Young's moduli ratios of inclusion to background with R^2 of 0.93. These results suggest that ST-HMI can contrast different stiffness inclusion. Though a 10 ± 1 mm diameter was targeted to image all inclusions, the perceived size varied between inclusions. This may be due to the difference in transducer pressure on the surface of the phantoms during imaging, use of

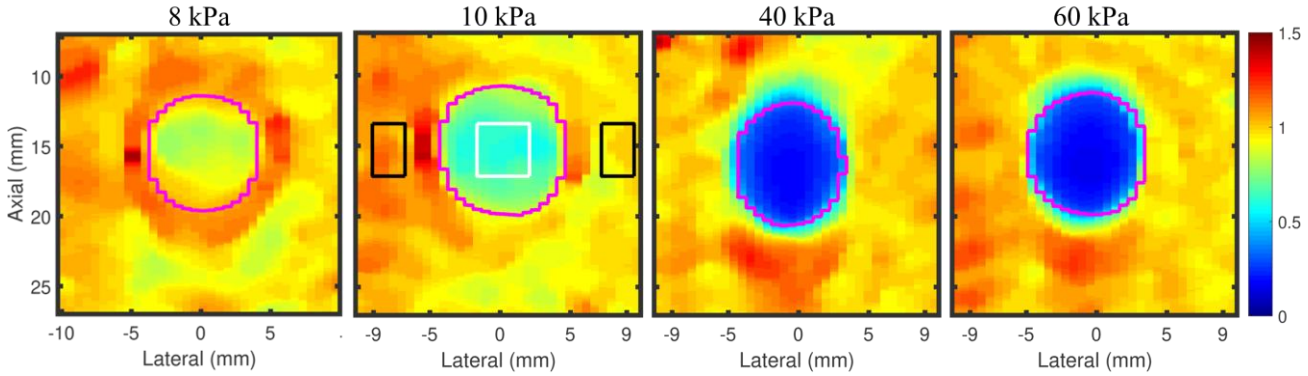

Fig. 2: ST-HMI derived normalized peak-to-peak displacement (P2PD) images of 8, 10, 40, and 60 kPa inclusions embedded in a 5-kPa background of two commercial phantoms. Magenta contour represents the inclusion boundary derived from the B-mode ultrasound image. Rectangular contours in the background (white) and inclusion (black) represent the region of interest for the comparison of P2PD ratio versus Young's modulus ratio, respectively.

the same oscillation frequency, and/or difference in true sizes. However, the perceived size was within the error range provided by the manufacturer.

In the preclinical mouse study, two observations were notable. First, the tumor grew over time. Second, P2P displacements at the tumor with respect to the non-cancerous tissue decreased over time. The P2PD ratio of non-cancerous tissue to the tumor was 2.0, 3.6, 7.0, and 6.6 at 1, 2, 3, and 4 weeks, respectively. One limitation of this analysis is the selection of ROI. As the non-cancerous tissue was not available at all axial depth (axial depth of around 8-11 mm), the axial ROI size was selected to cover the available background and maximum tumor in the lateral direction.

In the clinical study, the ST-HMI detected invasive ductal carcinoma (IDC) tumor from the surrounding non-cancerous breast tissue in a 54 yr. old patient. The median P2PD ratio of non-cancerous tissue to tumor was 1.78 in the patient. The size of the tumor was 4 mm. so, the St-HMI was able to detect as small as 4 mm tumor *in vivo*.

ST-HMI demonstrated very promising results in phantoms, mouse breast cancer model, and breast cancer patients. However, the study has three main limitations. First, P2PD displacements were used to infer mechanical properties. However, displacement is a function of both elasticity and viscosity [21]. Second, the P2PD ratio of non-cancerous tissue to tumor was used to account for the mouse to mouse variation in ARF amplitude. The mechanical property assessments will be confounded if the non-cancerous tissues experienced different force amplitude than the tumor or the mechanical properties of non-cancerous tissues change over time. Third, the mechanical anisotropy of breast tissues [22] was ignored. The mechanical anisotropy may confound the displacement measurements [23]–[25]. Future investigations will address these limitations.

IV. Conclusion

In this study, the initial feasibility of generating and tracking harmonic motion was shown using a single linear array transducer. ST-HMI contrasted four inclusions with varying stiffness using two commercially available phantoms. In the preclinical mouse study, the P2PD ratio of the tumor to non-cancerous tissues increased over time indicating that the relative stiffness of the tumor was increasing. In the clinical application, ST-HMI detected IDC and showed that the relative stiffness of IDC was higher than the surrounding non-cancerous tissue. These results indicate that ST-HMI is feasible and can assess the mechanical properties of tissue via generation and tracking of harmonic motion in the region of AM-ARF excitation.

Acknowledgment

This study was supported in part by NIH R01CA228275. The authors thank Drs. Saurabh Singh, Indranil Basu, and Chandan Guha from the Albert Einstein College of Medicine & Montefiore Medical Center, Bronx, NY USA for providing the cancer cell for the mouse experiments and Rachel Weber, Drs. Bret Taback, and Richard Ha for helping us collecting the breast cancer patient's data.

References

[1] R. M. S. Sigrist, J. Liau, A. El Kaffas, M. C. Chammas, and J. K. Willmann, "Ultrasound Elastography: Review of Techniques and Clinical Applications," *Theranostics*, vol. 7, no. 5, pp. 1303–1329, 2017.

[2] K. Nightingale *et al.*, "Derivation and analysis of viscoelastic properties in human liver: Impact of frequency on fibrosis and steatosis staging," *IEEE Trans. Ultrason. Ferroelectr. Freq. Control*, vol. 62, no. 1, pp. 165–175, 2015.

[3] R. Nayak, V. Kumar, J. Webb, A. Gregory, M. Fatemi, and A. Alizad, "Non-contrast agent based small vessel imaging of human thyroid using motion corrected power Doppler imaging," *Sci. Rep.*, vol. 8, no. 1, p. 15318, Dec. 2018.

[4] J. Zhan, J.-M. Jin, X.-H. Diao, and Y. Chen, "Acoustic radiation force impulse imaging (ARFI) for differentiation of benign and malignant thyroid nodules—A meta-analysis," *Eur. J. Radiol.*, vol. 84, no. 11, pp. 2181–2186, Nov. 2015.

[5] J. M. Correas *et al.*, "Prostate cancer: Diagnostic performance of real-time shear-wave elastography," *Radiology*, vol. 275, no. 1, pp. 280–289, Apr. 2015.

[6] M. M. Hossain *et al.*, "Mechanical Anisotropy Assessment in Kidney Cortex Using ARFI Peak Displacement: Preclinical Validation and Pilot In Vivo Clinical Results in Kidney Allografts.," *IEEE Trans. Ultrason. Ferroelectr. Freq. Control*, vol. 66, no. 3, pp. 551–562, Mar. 2019.

[7] M. M. Hossain *et al.*, "Evaluating Renal Transplant Status Using Viscoelastic Response (VisR) Ultrasound.," *Ultrasound Med.*

Biol., vol. 44, no. 8, pp. 1573–1584, May 2018.

[8] M. S. Taljanovic *et al.*, "Shear-Wave Elastography: Basic Physics and Musculoskeletal Applications," *RadioGraphics*, vol. 37, no. 3, pp. 855–870, May 2017.

[9] D. Marlevi *et al.*, "Combined spatiotemporal and frequency-dependent shear wave elastography enables detection of vulnerable carotid plaques as validated by MRI," *Sci. Rep.*, vol. 10, no. 1, p. 403, Dec. 2020.

[10] A. J. Collins *et al.*, "'United States Renal Data System 2011 Annual Data Report: Atlas of chronic kidney disease & end-stage renal disease in the United States.," *Am. J. Kidney Dis.*, vol. 59, no. 1 Suppl 1, pp. A7, e1-420, Jan. 2012.

[11] E. E. Konofagou and K. Hynynen, "Localized harmonic motion imaging: Theory, simulations and experiments," *Ultrasound Med. Biol.*, vol. 29, no. 10, pp. 1405–1413, 2003.

[12] T. Payen *et al.*, "Elasticity mapping of murine abdominal organs in vivo using harmonic motion imaging (HMI)," *Phys. Med. Biol.*, vol. 61, no. 15, pp. 5741–5754, Aug. 2016.

[13] T. Payen *et al.*, "Harmonic Motion Imaging of Pancreatic Tumor Stiffness Indicates Disease State and Treatment Response," *Clin. Cancer Res.*, vol. 26, no. 6, pp. 1297–1308, Mar. 2020.

[14] H. Chen *et al.*, "Harmonic motion imaging for abdominal tumor detection and high-intensity focused ultrasound ablation monitoring: an in vivo feasibility study in a transgenic mouse model of pancreatic cancer," *IEEE Trans. Ultrason. Ferroelectr. Freq. Control*, vol. 62, no. 9, pp. 1662–1673, Sep. 2015.

[15] Y. Han, S. Wang, T. Payen, and E. Konofagou, "Fast lesion mapping during HIFU treatment using harmonic motion imaging guided focused ultrasound (HMIgFUS) in vitro and in vivo," *Phys. Med. Biol.*, vol. 62, no. 8, pp. 3111–3123, Apr. 2017.

[16] J. Grondin, T. Payen, S. Wang, and E. E. Konofagou, "Real-time monitoring of high intensity focused ultrasound (HIFU) ablation of in vitro canine livers using harmonic motion imaging for focused ultrasound (HMIFU)," *J. Vis. Exp.*, vol. 2015, no. 105, pp. 1–7, Nov. 2015.

[17] S. Sadeghi, C.-Y. Lin, and D. H. Cortes, "Narrowband Shear Wave Generation Using Sinusoidally Modulated Acoustic Radiation Force," *IEEE Trans. Ultrason. Ferroelectr. Freq. Control*, vol. 66, no. 2, pp. 264–272, Feb. 2019.

[18] T. Savage, S. Pandey, and C. Guha, "Postablation Modulation after Single High-Dose Radiation Therapy Improves Tumor Control via Enhanced Immunomodulation," *Clin. Cancer Res.*, vol. 26, no. 4, pp. 910–921, Feb. 2020.

[19] A. Nabavizadeh *et al.*, "Noninvasive Young's modulus visualization of fibrosis progression and delineation of pancreatic ductal adenocarcinoma (PDAC) tumors using Harmonic Motion Elastography (HME) in vivo," *Theranostics*, vol. 10, no. 10, pp. 4614–4626, 2020.

[20] G. F. Pinton, J. J. Dahl, and G. E. Trahey, "Rapid tracking of small displacements with ultrasound.," *IEEE Trans. Ultrason. Ferroelectr. Freq. Control*, vol. 53, no. 6, pp. 1103–17, Jun. 2006.

[21] M. M. Hossain and C. M. Gallippi, "Viscoelastic Response Ultrasound Derived Relative Elasticity and Relative Viscosity Reflect True Elasticity and Viscosity: In Silico and Experimental Demonstration.," *IEEE Trans. Ultrason. Ferroelectr. Freq. Control*, vol. 67, no. 6, pp. 1102–1117, 2020.

[22] K. Skerl, S. Vinnicombe, K. Thomson, D. McLean, E. Giannotti, and A. Evans, "Anisotropy of Solid Breast Lesions in 2D Shear Wave Elastography is an Indicator of Malignancy," *Acad. Radiol.*, vol. 23, no. 1, pp. 53–61, Jan. 2016.

[23] M. Hossain, C. J. Moore, and C. M. Gallippi, "Acoustic Radiation Force Impulse-Induced Peak Displacements Reflect Degree of Anisotropy in Transversely Isotropic Elastic Materials," *IEEE Trans. Ultrason. Ferroelectr. Freq. Control*, vol. 64, no. 6, pp. 989–1001, Jun. 2017.

[24] M. M. Hossain and C. M. Gallippi, "Electronic Point Spread Function Rotation Using a Three-row Transducer for ARFI-Based Elastic Anisotropy Assessment: In Silico and Experimental Demonstration.," *IEEE Trans. Ultrason. Ferroelectr. Freq. Control*, vol. PP, no. c, pp. 1–1, Aug. 2020.

[25] M. Hossain and C. M. Gallippi, "On the feasibility of quantifying mechanical anisotropy in transversely isotropic elastic materials using acoustic radiation force (ARF)-induced displacements," in *Medical Imaging 2019: Ultrasonic Imaging and Tomography*, 2019, no. March, p. 12.